HHS Public Access

Author manuscript

*Aerosol Sci Technol*. Author manuscript; available in PMC 2015 October 26.

Published in final edited form as:

*Aerosol Sci Technol*. 2013 January ; 47(1): 81–92. doi:10.1080/02786826.2012.728301.

# Miniature Dual-Corona Ionizer for Bipolar Charging of Aerosol

**Chaolong Qi** and **Pramod Kulkarni**

Centers for Disease Control and Prevention, National Institute for Occupational Safety and Health, Cincinnati, Ohio, USA

## Abstract

A corona-based bipolar charger has been developed for use in compact, field-portable mobility size spectrometers. The charger employs an aerosol flow cavity exposed to two corona ionizers producing ions of opposite polarity. Each corona ionizer houses two electrodes in parallel needle-mesh configuration and is operated at the same magnitude of corona current. Experimental measurement of detailed charge distribution of near-monodisperse particles of different diameter in the submicrometer size range showed that the charger is capable of producing well-defined, consistent bipolar charge distributions for flow rates up to 1.5 L/min and aerosol concentration up to $10^7$ per $cm^3$. For particles with preexisting charge of +1, 0, and −1, the measured charge distributions agreed well with the theoretical distributions within the range of experimental and theoretical uncertainties. The transmission efficiency of the charger was measured to be 80% for 10 nm particles (at 0.3 L/min and 5 $\mu$A corona current) and increased with increasing diameter beyond this size. Measurement of uncharged fractions at various combinations of positive and negative corona currents showed the charger performance to be insensitive to fluctuations in corona current. Ion concentrations under positive and negative unipolar operation were estimated to be $8.2 \times 10^7$ and $3.37 \times 10^8$ $cm^{-3}$ for positive and negative ions; the $n{\cdot}t$ product value under positive corona operation was independently estimated to be $8.5 \times 10^5$ $s/cm^3$. The ion concentration estimates indicate the charger to be capable of "neutralizing" typical atmospheric and industrial aerosols in most measurement applications. The miniature size, simple and robust operation makes the charger suitable for portable mobility spectrometers.

## 1. Introduction

We report on the development of a bipolar charger for use in portable electrical mobility spectrometers for particle size distribution (PSD) measurement. Particle size measurement

Address correspondence to Pramod Kulkarni, Centers for Disease Control and Prevention, National Institute for Occupational Safety and Health, 4676 Columbia Pkwy, MS: R7, Cincinnati, OH 45226, USA. PSKulkarni@cdc.gov.

The findings and conclusions in this report are those of the authors and do not necessarily represent the views of the National Institute for Occupational Safety and Health. Mention of a product or company name does not constitute endorsement by the Centers for Disease Control and Prevention.

Supplemental Information: Supplemental information and data are available online on the journal website on the following topics: (1) a picture of a DCBC prototype; (2) uncharged fraction of 100 nm test particles as a function of time over extended periods of operation; (3) example of charge distribution of 100 nm test particles obtained from DCBC; (4) estimation of uncertainty associated with measurement of charge distribution; (5) mobility size distributions obtained using different neutralizers for negative and positive polarity of the DMA electrode; (6) PSD obtained using DCBC and $Kr^{85}$ at different relative humidity of test aerosol; (7) uncharged fraction from the DCBC as a function of corona currents; (8) Charge distributions of 100 nm particles (with no preexisting charge) corresponding to different configurations of positive and negative corona currents at an aerosol flow rate of 0.3 L/min; and (9) intrinsic and extrinsic charging efficiency of 20 nm particles when operated as a unipolar charger.

using electrical techniques relies on the use of *a priori* known charge on the particles. Most aerosols acquire distribution of electrical charge when exposed to ions and electrons. Knowing the fraction of particles of a given size that carry a given number of charges is an essential step for any electrical measurement technique. Production of known charge distribution is generally achieved by passing the aerosol through either a unipolar charger that applies same polarity (positive or negative) to all particles, or a bipolar diffusion charger which produces a population containing particles with positive, negative, and no electrical charge.

Early mobility techniques employed unipolar chargers; for example, the electrical aerosol analyzer (Liu and Pui 1975) used a unipolar charger to attain high charging efficiencies to allow measurement of particles. However, charge distribution acquired by an aerosol in a unipolar charger is a strong function of the variation in flow residence time, ion properties and abundance, preexisting charge on particles, and particle properties. This led to preferential use of bipolar chargers for mobility measurements due to the “equilibrium” distribution produced by bipolar chargers and their relative insensitivity to variation in flow conditions, preexisting charge, and aerosol properties. Use of bipolar chargers is also desirable to reduce the degree of multiple charging, which can be substantially higher in unipolar charger particularly for larger particles. Reduced multiple charging in bipolar chargers has allowed extending mobility-based size measurements with good precision up to 1 $\mu$m diameter.

Most mobility size spectrometers today use radioactive ionizers to produce equilibrium, bipolar charge distribution of sampled aerosols. However, regulatory restrictions on the use of radioactive sources have prevented mobility spectrometers employing these chargers from being used in many field studies. This has motivated several investigators to develop new charger designs that do not employ radioactive sources, but still produce quasi-equilibrium charge distributions. Adachi et al. (1993) developed a bipolar charger by using two corona ionizers, one for positive and one for negative ions. A large particle-free flow at high pressure was used to drive the ions from the corona regions into an opposing-jet mixer and a subsequent charging chamber, where the ion flows were mixed with each other and the incoming aerosol flow to be neutralized. Romay et al. (1994) further provided a modified design using a similar concept of the sonic jet ionizer. However, these approaches require an additional flow for ion transport (increasing the complexity of the charger operation), and lead to significant dilution of the aerosol flow. Also, in this type of bipolar charger, the ratio of positive to negative ion concentration must be actively balanced by careful adjustments of the corona ionizers in order to provide equilibrium charge distributions. This considerably increases the complexity of the device. Many other alternative approaches using AC corona discharge (Zamorani and Ottobrini 1978; Stommel and Riebel 2004), soft X-ray photoionization (Shimada et al. 2002), and surface dielectric barrier discharge (Kwon et al. 2005) have been developed that eliminate the need for ion transport flow and dilution problems. However, these approaches involve either considerable degree of complexity with respect to their operation or rely on bulky, large, or expensive hardware that prevents their use in field-portable, compact instrumentation.

The objective of our study was to develop a compact, miniature, low-cost bipolar charger for use in portable, hand-held mobility size spectrometers. In addition to providing consistent, well-defined bipolar charge distribution, the following physical attributes of the charger were desirable with respect to their use in hand-portable field instrumentation: (i) compact and miniature in size, (ii) free of radioactive sources allowing access to any field site, (iii) simple and robust operation that does not use additional dilution or sheath flows, and (iv) low-cost and easy to construct. While many of the above physical attributes can be readily met by a suitably designed (for hand-held instrumentation) unipolar charger, a key motivation for using a bipolar charger was to allow measurement over the entire sub-micrometer size range. Use of a unipolar charger for mobility size distribution measurement can lead to large uncertainties for particles larger than 300–400 nm (Qi and Kulkarni 2012). On the other hand, a bipolar charger can permit mobility size measurements over extended size range with lower uncertainties. We have developed a new charger using dual coronas that largely meets the abovementioned needs. This article discusses design and experimental characterization of our dual-corona bipolar charger (DCBC).

## 2. Experimental

### 2.1. Charger Design

The design and the electrical and analog signal I/O connections of our DCBC are illustrated in Figure 1. The miniature device (1.9 cm × 1.6 cm × 1.9 cm) incorporates a simple and symmetric design, which enables its use in a wide range of aerosol charging and neutralizing applications. Figure 1 shows the schematic drawing and Figure S1 in the online supplementary information shows an actual picture of the prototype DCBC. The dielectric parts of the prototype were machined using polyvinyl chloride (PVC; dielectric constant: 3.0) for electrical insulation. Fabrication of the charger parts using a 3D printer (Dimension 3D uPrint Plus, Stratasys, Inc., MN, USA) with Acrylonitrile butadiene styrene (ABS; dielectric constant: 2.0–3.5), which can dramatically reduce fabrication time and costs, were also explored. As shown in Figure 1, the design incorporates a cylindrical metal tube made of aluminum (inner diameter of 1.6 mm) that carries the aerosol flow, with two identical corona ionizers, facing each other, positioned symmetrically about the aerosol flow axis. Each corona ionizer is housed in a dielectric cavity and consists of a sharp tungsten high voltage (HV) electrode and a metal mesh held at virtual ground. The axis of the tungsten electrode, which has a diameter of 250 $\mu$m with a tip diameter of 5 $\mu$m, is kept parallel to the plane of the grounded mesh with a distance of about 1.5 mm (from the axis of the tungsten electrode to the surface of the grounded mesh). This parallel orientation was preferable to needle-to-plane configuration as it was relatively easier to maintain a fixed distance between electrode axis and the mesh. The grounded mesh electrode was made of a fine stainless steel screen. Two types of mesh electrodes were tested: one with higher open area of about 80% and a square opening of 350 $\mu$m, and the other with a lower open area of about ∼38% and a round opening of 280 $\mu$m. No apparent difference on the charging performance was observed. The experimental data presented here correspond to the mesh with an open area of 80%. The distance between the two mesh electrodes was approximately 9 mm.

One ionizer is operated to produce positive corona discharge, and the other to produce negative discharge. Therefore, one ionizer produces positive ions and the other produces negative ions. The ion flux from each corona ionizer was indirectly controlled by controlling the corona current in each ionizer module via proportional–integral–derivative (PID) controller. The electrical and analog signal I/O connections and the PID control used to operate the two ionizers are also shown in Figure 1 (the entire electronic circuitry can be accommodated on a small printed circuit board measuring a few tens of $cm^2$). Typically, the variation in corona current was less than ±10% about the set point value during steady operation. The potential difference between the grounded mesh electrodes of the two opposite ionizers was measured to be about 1–3 mV during steady operation under PID control. Aerosol was exposed to the positive and negative ions from each ionizer module using a round opening (5.1 mm in diameter) located in the center of the aerosol flow tube (referred to as “flow cavity” in Figure 1). The electric field resulting from the voltage drift between the two mesh electrodes was too insignificant to affect the transport of ions or particles in the flow cavity over typical timescales for these processes. The overall assembly is air-tight, and all electrical connections are made from the outside. The design offers considerable ease of fabrication and use. The current charger design and operation was optimized for low aerosol flow rate of ∼0.3 L/min for use in a portable mobility spectrometer.

### 2.2. Charger Characterization

The experimental setup for charger characterization is shown in Figure 2. The performance of the DCBC was evaluated using both silver nanoparticles (smaller than 50 nm) and polystyrene latex (PSL) particles (50 nm and larger). For silver nanoparticles, the test aerosol was produced using a tube furnace as an evaporation-condensation particle generator. A pneumatic atomizer (Model 3076; TSI Inc., Shoreview, MN, USA) or an electrospray aerosol generator (Model 3480; TSI Inc., Shore-view, MN, USA) was used to atomize an aqueous suspension of PSL microspheres of different sizes (Duke Scientific, Palo Alto, CA, USA) for producing the PSL test aerosol. Test aerosols from different aerosol generators were subsequently classified in a differential mobility analyzer (DMA, Model 3081 and 3085; TSI Inc., Shoreview, MN, USA; operating at a 10:1 sheath-to-aerosol flow ratio) to provide monodisperse test particles. By changing the polarity of the power supply of the DMA, charged test particles carrying positive or negative charges were obtained. To obtain uncharged test particles, the DMA-classified aerosol was neutralized by a $Po^{210}$ charger, followed by removal of remaining charged particles in an electrostatic precipitator (ESP1 in Figure 2). The number concentration of DMA-classified aerosol in all charging experiments was lower than $10^5$ per $cm^3$, ensuring adequate ion-to-particle concentration ratio needed for equilibrium charging.

Using the above-mentioned test aerosols, the uncharged fraction ($f_0(d_p)$), charge distribution ($f_i(d_p)$), and transmission efficiency ($P(d_p)$) of the DCBC were characterized. The uncharged fraction ($f_0(d_p)$) denotes the percentage of particles that have diameters $d_p$ and are uncharged after passing the bipolar charger; and the transmission efficiency ($P(d_p)$) represents the percentage of particles with diameters $d_p$ that penetrate through the charger. In the experimental setup, a second electrostatic precipitator (ESP2 in Figure 2) was used

downstream of the DCBC to remove the charged particles. An ultrafine condensation particle counter (UCPC, Model 3025A, TSI Inc., Shoreview, MN, USA) was then used to measure the number concentration of the particles. The flow rate through the DCBC was varied and controlled by the pump in the UCPC together with a mass flow controller (MFC) as shown in Figure 2. Using the particle concentrations measured under different conditions, the uncharged fraction ($f_0(d_p)$) and transmission efficiency ($P(d_p)$) can be obtained using the following equations:

$$f_0(d_p)=\frac{N_2}{N_1} \quad [1]$$

$$P(d_p)=\frac{N_4}{N_3} \quad [2]$$

where $N_1$ is the number concentration of particles of size $d_p$ downstream of the ESP2 with both coronas operating and the ESP2 off; $N_2$ is the particle number concentration downstream of the ESP2 with both coronas operating and the ESP2 on; $N_3$ and $N_4$ are the particle number concentrations upstream and downstream of the DCBC, respectively.

Particle charge distribution function $f_i(d_p)$ is a frequency function describing the fraction of the total number of particles of diameter $d_p$ carrying $i$ charges, where $i$ is an integer from $-\infty$ to $+\infty$ (−4 to +4 in this experimental study). After passing the DCBC, the electrical mobility distribution of the monodisperse test particles was measured by a scanning mobility particle size spectrometer (SMPS, Model 3936, TSI Inc., Shoreview, MN, USA) without using its native $Kr^{85}$ bipolar charger (Model 3077, TSI Inc., Shoreview, MN, USA). Since the test particles are monodisperse in size, the measured electrical mobility distribution represents the particle charge distribution. Positive and negative power supplies for the DMA in the SMPS were used alternately such that the complete charge distribution function $f_i(d_p)$ could be retrieved using the measured $f_0(d_p)$ from the uncharged fraction experiments. As the positive and negative charge distributions were measured separately, total number concentrations of particles exiting the charger were also recorded by a UCPC before and after each SMPS measurement to make the positive and negative charge distributions comparable. Thus, the charge distribution function $f_{+i}(d_p)$ for positively charged particles can be obtained by using the following equation:

$$f_{+1}(d_p)=\left(1-f_0(d_p)\right)\cdot\left(\frac{\frac{\sum_i N_i^+}{N_{\text{tot}}^+}}{\frac{\sum_i N_i^+}{N_{\text{tot}}^+}+\frac{\sum_i N_i^-}{N_{\text{tot}}^-}}\right)\cdot\frac{N_i^+}{\sum_i N_i^+} \quad [3]$$

where, $N_i^+$ is the total number of particles carrying $+i$ charges obtained by integrating the peak (corresponding to $+i$ charge) in the mobility distribution obtained using negative potential on the DMA central electrode ( $N_i^-$ is the corresponding term for negatively charged particles); $\sum_i N_i^+$ is the total number of particles in a mobility distribution obtained

using negative polarity of central electrode of DMA ( $\sum_i N_i^-$ is the corresponding term for positive polarity of central electrode of DMA); $N_{\text{tot}}^+$ and $N_{\text{tot}}^-$ are total number concentration of aerosol at the outlet of the charger corresponding to positive and negative DMA electrode polarity scans. $N_{\text{tot}}^+$ and $N_{\text{tot}}^-$ were obtained by averaging CPC concentrations at the outlet of the charger (over 30 s sampling time) before and after every mobility distribution measurement using positive or negative polarity in the DMA, respectively. In principle, $f_{+i}(d_p)$ above can be retrieved just based on the measurement of $N_i^+$, $N_i^-$, $\sum_i N_i^+$; however, we based it on the measured $(1 - f_0(d_p))$ because this quantity was directly measured with highest precision in our experiments. For an ideal case, where the concentration of the test aerosol does not fluctuate with time, $N_{\text{tot}}^+ = N_{\text{tot}}^-$, Equation (3) reduces to,

$$f_{+i}(d_p) = (1 - f_0(d_p)) \cdot \frac{N_i^+}{\sum_i N_i^+ + \sum_i N_i^-} \quad [4]$$

Similar equations can be written for the charge distribution of negatively charged particles. Normalizing measured fractions with $N_{\text{tot}}^+$ and $N_{\text{tot}}^-$ in Equation (3) helps account for fluctuations in inlet aerosol concentrations during mobility distribution measurement, as well as over the time duration required to switch the polarity of DMA power supplies. Also, the measurement uncertainty associated with charge distribution given by Equation (3) was calculated using propagated uncertainties and is described in the supplementary information.

To estimate the ion concentration in the charger, ion current across two parallel electrodes in an electrostatic precipitator (located immediate downstream of the charger) was measured using an electrometer (Model 6514, Keithley Corp., Cleveland, OH, USA). The charger was sequentially operated in positive and negative unipolar mode (with only one corona ionizer operating, the other turned off). The ion concentration downstream of the charger was estimated using the equation: $n = I/Qe$, where $n$ is the ion concentration, $I$ is the electrical current measured by the electrometer, $e$ is the elementary charge, and $Q$ is the flow rate.

## 3. Results

### 3.1. Performance Characterization of the DCBC

Experiments were conducted to measure (i) total uncharged fraction of particles at the outlet of the bipolar charger (ii) detailed charge distribution on aerosol particles, (iii) transmission efficiency of particles through the charger, and (iv) size distribution using DCBC and other reference chargers. The aerosol flow rate in the DCBC was maintained at 0.3 L/min and the two ionizers were operated at corona currents of +5 and −5 $\mu$A. The voltage–current (V–I) characteristics of each ionizer were found to be independent of each other—that is V–I characteristics of one corona module was not affected by the operational characteristics of the other corona module and vice versa. Under steady-state operating conditions, ozone concentration at the outlet of the charger was measured (using a UV photometric ozone monitor; Model 205, 2B Technologies, Inc., Boulder, CO, USA) to be 540 ± 26 ppb at abovementioned corona currents and flow rates. Measurements using a UCPC confirmed that no particles (larger than about 3 nm, corresponding to the lower detection limit of the

UCPC) were detected during the operation of either single or dual coronas in the charger. There is a remote possibility of particle formation in the corona discharge. However, it is highly unlikely that the particles produced in the corona will be entrained in the aerosol flow, because both corona discharges are completely isolated from the aerosol flow path. Measurements using a UCPC confirmed that no particles (larger than about 3 nm, corresponding to the lower detection limit of the UCPC) were detected during the operation of either single or dual coronas in the charger. This ensured that there was no interference from corona-generated particles, if any, in the measurement of charge distribution.

**3.1.1. Uncharged Fraction ($f_0(d_p)$)—**Figure 3 shows uncharged fraction ($f_0(d_p)$) measured downstream of the DCBC for three types of monodisperse aerosol, each carrying a different preexisting charge: +1, 0, and −1. The error bar around each data point in Figure 3 represents the propagated measurement uncertainty defined in Equation (S1) in the online supplementary information. Also plotted, for comparison, are the uncharged fractions from theoretical approaches—one using the Boltzmann statistics (Keefe et al. 1959) and the other from combined Fuchs (1963) and Gunn (1956) approach, which will hereafter be referred to as Fuchs–Gunn theory. The results from Fuchs approach were calculated using parameterization given by Wiedensohler (1988)—after accounting for the corrected ion-particle collision probability of Hoppel and Frick (1986). Corrected coefficients for $a_{4,1}$ and $a_{5,2}$ in Wiedensohler's approximation were used (Flagan 2011). Fraction of particles with charge level 3 or higher, were obtained using Gunn (1956) model. In the Gunn model, a positive to negative ion mobility ratio of 0.875 was used (Wiedensohler et al. 1986). Figure 3 clearly shows that the uncharged fraction for all aerosols, including the ones with preexisting charge, agrees well—within the experimental uncertainty—with that from the equilibrium Boltzmann and Fuchs–Gunn theories. For particles smaller than 50 nm, the uncharged fraction calculated from the Fuchs-Gunn theory are lower compared to those from the Boltzmann statistics by 3.4% at 50 nm and 8.1% at 10 nm. It is worth noting that the measured uncharged fractions from our charger are in between these two theoretical values for particles below 50 nm. The propagated uncertainty of measurement (as represented by the error bar) is about 4.0% at 10 nm and 2.2% at 50 nm. Figure S2 shows uncharged fractions of 100 nm particles measured over 8-h continuous operation period. The data demonstrate that the charger is capable of producing consistent charge distributions over extended time periods of operation.

Figure 4 shows the effect of flow residence time on the charger performance. Influence of the residence time on charger performance was investigated to probe the onset of nonequilibrium charging conditions. With the two corona ionizers operating at +5 and −5 $\mu$A corona currents, the uncharged fraction of 20 nm particles under different flow rates were measured and are shown in Figure 4. The equilibrium charging behavior is clearly evident in Figure 4 below 1.5 L/min, corresponding to approximately 2 ms residence time, with uncharged fractions being constant (within the experimental uncertainty) and close to those from the Fuchs–Gunn theory—even for particles with different preexisting charge states. This is consistent with the data in Figure 3. As the aerosol flow rate increases beyond 1.5 L/min, the uncharged fractions start to deviate from the equilibrium values. These data

indicate that the current charger should be operated at flow rates below 1.5 L/min at 5 $\mu$A corona current, to obtain equilibrium charge distributions.

**3.1.2. Charge Distribution ($f_i$)—**Particle charge distribution was measured for monodisperse test particles ranging from 10 to 500 nm in diameter. Figure S3 presents the charge distribution data for 100 nm test particles with different preexisting charge states. The charge distributions calculated from Boltzmann statistics (solid curve) and Fuchs-Gunn theory (dashed curve) are also shown for comparison. Boltzmann distribution is symmetric while the distribution from Fuchs–Gunn theory, as expected, is asymmetric due to the higher electrical mobility of negative ions. As shown in Figure S3, the experimentally measured charge distributions, including those with the preexisting charge, from our charger agree very well with the theoretical charge distributions.

Complete charge distribution data for all monodisperse test particles obtained in this work are presented in Figure 5a–c corresponding to aerosol with preexisting charge of +1, 0, and −1, respectively. These figures show fraction of particles with a given charge level ($f_i$) as a function of diameter ($d_p$). Theoretical charge distributions for both positive and negative fractions from Fuchs–Gunn theory are also shown. In general, the experimental charge distributions from DCBC, regardless of the preexisting charge states on the sampled particles, agree well with those from the Fuchs–Gunn theory. Propagated measurement uncertainties, represented by the error bars, which were calculated using Equations (S3) and (S4, are amplified at smaller particle sizes (<20 nm) and for measurement of higher charge fractions (>2). Below 20 nm, for particles with negative preexisting charge, the measured fractions for singly charged particles seem to be consistently lower than that expected from Fuchs–Gunn theory. Even at flow rate of 0.3 L/min, the residence time of particles in the charger may not be adequate to achieve equilibrium charge distribution of smaller particles.

**3.1.3. Transmission Efficiency ($P(d_p)$)—**The transmission efficiency of DCBC was experimentally characterized and is shown in Figure 6. The top and bottom panels of Figure 6 show the experimental data with the two ionizers of the DCBC turned on and off, respectively. When the two ionizers were off, the particle loss in the DCBC is mainly due to particle diffusion in the submicrometer range. As shown in the bottom panel of Figure 6, the diffusion loss is very small; the transmission efficiency is more than 90% for all the test particles in the diameter range of 10 to 500 nm. When the two ionizers were turned on, as shown in the top panel of Figure 6 the particle transmission efficiency decreased, especially for smaller particles. For 10 nm particles, the transmission efficiency was approximately 80% at 0.3 L/min, and was greater than 90% for particles larger than 100 nm. Figure 6 also shows the negligible effect of preexisting charge level of the test particles on their transmission efficiency. At 10 nm, the neutral particles have higher penetration compared to those with preexisting charge of +1 or −1, suggesting enhanced losses, perhaps due to image forces or space charge effect (though there would be no space charge in an ideal bipolar ion atmosphere, its existence can not be ruled out in our charger where relatively inhomogeneous regions may exist close to each ionizer). A slight, but finite, potential difference between the two mesh electrodes (<3 mV) is unlikely to cause significant migration velocities of particles smaller than 10 nm in diameter to result in enhanced losses.

The experimental data from different preexisting charge states were averaged for each particle size and a best fit was obtained to describe mean size-dependent penetration efficiency of our charger. The best fit can be used to calculate the particle transmission efficiency at 0.3 L/min aerosol flow rate and +5 and −5 $\mu$A corona currents in the two corona ionizers.

**3.1.4. Comparison with Other Bipolar Chargers—**Experiments were conducted to compare the overall ability of charge-conditioning of our bipolar charger with that of the other commercial $Kr^{85}$ (Model 3077, TSI Inc., Shoreview, MN, USA) and Soft X-Ray (Model 3087, TSI Inc., Shoreview, MN, USA) bipolar chargers. Polydisperse NaCl particles were produced by atomizing an aqueous NaCl solution using a pneumatic atomizer followed by desolvation of droplets in a diffusion dryer. The aerosol generated from atomizer could acquire some charge distributions during the atomization process; therefore, it was passed through a $Po^{210}$ neutralizer followed by an ESP (to remove all charged particles) to obtain uncharged aerosol. The size distribution of the uncharged test aerosol was then measured using the scanning mobility spectrometer equipped with one of the three bipolar chargers and was compared with each other. In this experiment, all the three bipolar chargers were operated at a 0.3 L/min flow rate and the DCBC was operated at +5 and −5 $\mu$A corona currents.

Figure 7 shows PSD scans corresponding to both negative and positive voltage of the central electrode in the DMA, corresponding to classification of positively and negatively charged populations of the test aerosol. The *y*-axis represents raw number count in each size bin, and the *x*-axis represents mobility diameter. Each PSD curve represents the average over three replicate measurements. The repeatability of the PSD data was excellent with the standard deviation being only 0.4% of the average value at the peak diameter of the PSD (error bars not shown in Figure 7 for clarity). The particle transmission efficiency of DCBC (i.e., data in Figure 6) was accounted for in Figure 7. The transmission efficiency of TSI 3077 neutralizer was close to 100% (Covert et al. 1997); whereas for the soft X-ray ionizer, it was assumed to be 100% in the absence of any data.

As shown in Figure 7, when the DMA voltage is negative (i.e., for positively charged population), all three chargers produce size distributions that are in good agreement. Size distributions from the DCBC and $Kr^{85}$ are almost identical, with the soft X-ray charger giving slightly higher concentration at the modal diameter. In the case of a positive voltage on the DMA (i.e., for negatively charged population), the $Kr^{85}$ source gives slightly higher concentration at the peak compared to the other two chargers. The difference in number concentration from DCBC and $Kr^{85}$ is about 0.4% at the peak diameter, and that between the soft X-ray and $Kr^{85}$ is about 1.8%. For both the DCBC and the soft X-ray charger, the PSDs corresponding to the positively and negatively charged populations were similar; however, for $Kr^{85}$source, the number concentrations of negatively charged population were slightly higher. Test aerosol with preexisting charge (aerosol from the atomizer without passing the $Po^{210}$ neutralizer and the ESP) was also used to further probe the “neutralizing” potential of our charger; the results are presented in Figure S4, which shows that the size distributions obtained using our charger agree well with those from the radioactive ionizer. It is worth noting that the total number concentration of the test polydisperse aerosol was in

the range of $10^6$ to $10^7$ per $cm^3$. Coagulation can lead to growth of aerosol, particularly in the two commercial ionizers due to their larger volumes and residence time. However, order-of-magnitude analysis using the aerosol number concentrations and residence times—which were on the order of few seconds for $Kr^{85}$ and soft X-ray chargers—shows that the size distribution shift by coagulation is unlikely. Nonetheless, the results suggest that DCBC, operated at the specified conditions, is capable of charge-conditioning an aerosol below this concentration range.

The performance of the charger at different relative humidity of the test aerosol was also investigated; the data are shown in Figure S5. The main objective was to probe the relative sensitivity of corona characteristics and the resulting charge distributions to the variation in moisture content of the aerosol. The corona operation was found to be stable over the range of humidity tested (∼25–84%). The coronas at 5 $\mu$A current were found to be unstable at humidity nearing 100%. At such high humidity, the corona ionizers should be operated at lower corona currents for stable operation. There is a slight change in size distributions due to increased humidity as seen in Figure S5. The peak of the distribution from our charger shifts slightly to the left, by about 22.3% (26.2 nm), when the relative humidity increases from 25 to 84%; however, the peak concentration remains nearly the same. Also worth noting is qualitatively similar behavior of $Kr^{85}$, which also showed a shift in distribution at higher humidity, though unlike the DCBC the peak concentration increased by 32% at higher humidity.

### 3.2. Sensitivity of Charging Characteristics to Corona Currents

As described earlier, the corona current in each ionizer was maintained at a constant value using a PID controller. We probed the influence of the magnitude of the corona current in each ionizer on the charging characteristics. Figure S6 shows the uncharged fraction of 10 nm (top panel) and 100 nm (bottom panel) particles at 0.3 L/min flow rate. The two corona ionizers were operated at identical corona currents ranging from 2 to 8 $\mu$A, shown on *x*-axis in Figure S6. As shown in the figure, the effect of the magnitude of corona current on the uncharged fraction is generally insignificant within the range of experimental uncertainties. At 2-$\mu$A corona current, the uncharged fraction for 10 nm particles, carrying +1 preexisting charge, is lower than that from both Boltzmann statistics and Fuchs–Gunn theory, possibly due to inadequate ion concentrations required to achieve equilibrium in a given time.

Figure 8 presents the effect of corona current on transmission efficiency of 10 nm (top panel) and 100 nm (bottom panel) particles under similar operating conditions used in Figure S6. The transmission efficiency generally decreases with increasing corona current; the effect is more pronounced for smaller particles with preexisting charge. Results in Figures S6 and 8 suggest that operating the charger at corona currents of +5 and –5 $\mu$A is optimum for obtaining reliable charge distributions.

We also investigated the sensitivity of charge-conditioning performance of our charger to variation in corona currents in either of the two modules. The two ionizers were operated at different magnitudes of corona currents; the uncharged fractions ($f_0(d_p)$) of 100 nm particles were measured at the following configurations of corona currents in the two ionizers: (+2, −2 $\mu$A), (+2, −8 $\mu$A), (+8, −2 $\mu$A), and (+8, −8 $\mu$A). The uncharged fractions and the charge

distributions of 100 nm particles shown in Figures 9 and S7 in the supplementary information imply that the charge distributions are not a strong function of magnitude of corona current in each ionizer. This suggests that the ion concentration ratio in the flow cavity is a weak function of the magnitude of corona current (within the range studied) in the two ionizers.

## 4. Discussion

Results presented in Figures 3, S3, 5, and 7 clearly demonstrate the ability of our DCBC to consistently provide well-defined, near-equilibrium charge distributions of particles in the size range 10–500 nm. Though not studied in this work, similar near-equilibrium charging characteristics are expected for larger particles. The measured charge distributions, for aerosols with preexisting charge levels, generally agreed well, within the range of experimental uncertainty, with those expected from the Fuchs–Gunn theory. More importantly, the charge distributions obtained were well-defined and reproducible. The only significant systematic deviation was the lower charge fractions for particles smaller than ∼20 nm with preexisting charge of −1, which could perhaps be attributed to inadequate residence time or ion concentration. Providing a higher residence time, could perhaps allow attaining equilibrium charge distribution for very small particles. We expect that the charger would be appropriate for bringing typical atmospheric and workplace aerosols to a consistent, well-defined, steady-state charge distribution.

While it is desirable that the charge distribution of aerosol in any bipolar charger be determined solely by the diffusion charging dynamics in an “ideal” bipolar atmosphere, in reality the charge distributions obtained from most ionizers depend on the ionizer design and downstream plumbing geometry as demonstrated by Hoppel and Frick (1990). Their experiments with commonly used alpha and beta particle ionizers showed that the most ionizers do not achieve equilibrium charge distribution due to, among other factors, a region of unequally decaying ionic concentrations, leading to an ion imbalance downwind of the radioactive source. In this region, nonequilibrium conditions persist and the ratio of ion concentration continuously changes due to diffusion loss of ions to the walls and the mutual interaction of ion clouds. Covert et al. (1997) have also demonstrated the inability of commonly used $Kr^{85}$ ionizer (model 3077, TSI Inc., Shoreview, MN, USA) to apply equilibrium charge distribution at typically used range of concentrations and flow rates. Even though many common radioactive ionizers may not provide “true” equilibrium charge distributions, the uncertainty introduced by their nonequilibrium character, has been largely acceptable for most measurement applications. In this context, the range within which our experimental data quantitatively agrees with the theoretical equilibrium distributions can indeed be considered acceptable.

It is apparent from the well-defined charge distributions obtained from our charger, that there exists an almost-equal and consistent polar ion concentration in the aerosol flow path. However, it is not clear what mechanisms are responsible, in the absence of any “applied” electric field, for ion transport across the mesh electrodes into the flow cavity. We have also noted in an earlier study, involving unipolar charger with similar electrode configuration (Qi and Kulkarni 2012), that a constant ion transport into the aerosol flow can be obtained

across the grounded mesh in the absence of any bias voltage. We surmise that this phenomenon could be attributed to the fluid flow across the mesh electrodes from electrohydrodynamic (EHD) perturbations between corona and mesh electrodes during sustained corona generation. Strong ionic or electric wind has been reported crossing the mesh electrode at high velocities, in geometries with similar electrode configuration (Withers and Mecher 1981; Bequin et al. 2003).

In our charger, the same magnitude of corona current is maintained in both ionizer modules with the expectation that this will lead to identical ion transport flux into the aerosol flow; however, ion concentration measurements discussed later indicate this to be not a critical condition. Moreover, the charge distribution data in Figures 9 and S7 suggest that the ratio of ion concentrations in the flow cavity is not a strong function of relative difference in corona currents in the two modules. This is somewhat counterintuitive, and perhaps practically valuable finding, as it implies robust operation under small fluctuations in the corona current. As the ion clouds emerge from each corona ionizer, the ions experience repulsive Coulomb interaction (space charge effect) as well as attractive Coulomb interactions with the ions (of opposite polarity) from the opposing ionizer. These mutual interactions result in the migration of both polarity ions toward each other, and subsequent entrainment into the aerosol flow, where they create a bipolar ion atmosphere. It is plausible that any imbalance in the ratio of the two polar ion concentrations creates an electric field (following Gauss' law electric field is proportional to the charge enclosed within the volume), which in turn, quickly acts to offset the imbalance, thereby leading to near-equal ion concentrations. This may partially explain the low sensitivity of corona current variation to uncharged fractions measured in the experiments. In radioactive ionizers, Hoppel and Frick (1990) have also noted that in a region of high volume ionization, the polar ion concentrations generally remain equal.

We made an effort to estimate the range of ion concentration in the charger. A single ionizer module was operated in a “unipolar” mode and ion current was measured immediately downstream of the charger using an electrostatic precipitator. Ion currents of 36 and 140 pA were measured for positive and negative corona respectively, at 0.3 L/min and 5 $\mu$A corona current in ionizer. Based on the measured ion current and flow rate, ion concentration of $6.75 \times 10^7$ and $2.63 \times 10^8$ per $cm^3$ were estimated for positive and negative corona respectively at the exit of the DCBC. Assuming the electrical mobility to be 1.33 and 1.84 $cm^2/V$ s for positive and negative ions (Hoppel and Frick 1990) respectively, their respective diffusional losses to the walls of the transport tubing downstream of the flow cavity were estimated to be approximately 30 and 36% at 0.3 L/min (the actual loss could be somewhat higher due to image forces and space charge effect). By taking the average of the ion concentrations at the exit and inside the flow cavity of DCBC, the average positive and negative ion concentrations are estimated to be $8.2 \times 10^7$ and $3.37 \times 10^8$ per $cm^3$.

As an alternate method, $n \cdot t$ value of the charger was also estimated using the charging efficiency in the “positive unipolar” mode. As above, only one corona module was turned on and no potential was applied to the corona electrode in the other module (it was turned off). With the mesh electrodes in both ionizers at the identical ground potential, the charging efficiency of initially uncharged 20 nm particles in the “positive unipolar” mode was

determined to be 12% at 0.3 L/min aerosol flow rate and 5 $\mu$A corona current. Figure S8 shows charging efficiency data in the unipolar mode as a function of bias voltage (applied to the opposite mesh electrode). An "apparent" $n{\cdot}t$, derived from fitting the Fuchs numerical model to this charging efficiency (12% at a bias voltage of zero) by treating $n{\cdot}t$ as a fitting parameter, was found to be $8.5 \times 10^5$ s/cm$^3$. At 0.3 L/min flow rate, flow residence time is estimated to be 2 ms in the flow cavity and 11 ms including the downstream ion-mixing region (Figure 1). Using a flow residence time of 11 ms for the charger, the average ion concentration ($n$) inside the charger is estimated to be $7.73 \times 10^7$ per cm$^3$ at the established $n{\cdot}t$ value. This is within 6% of the value estimated above using ion currents, indicating reasonable agreement between the two methods.

The ion concentrations of positive and negative ions estimated above differ by a factor of ~4, in spite of identical corona currents. The reasons for this large difference are not known; we suspect that this could be due to markedly different characteristics of EHD or electric wind in positive and negative coronas that ultimately lead to different ion concentrations in the flow chamber. However, it is not clear if the estimated "unipolar" values are representative of *in-situ* concentrations in the flow cavity under "bipolar" operation. If anything, the measured charge distribution data suggest equilibrium charging characteristics implying near-equal polar ion concentrations. This further implies that if the ion concentrations (resulting from ion flux from each ionizer) are dissimilar, they perhaps quickly reach similar values as a result of the interplay between Coulomb attraction, space charge effect, and diffusional losses. One can arbitrarily assume that the lowest ion concentration of $8.2 \times 10^7$ per cm$^3$ estimated above represents the equilibrium value for both polar ion concentrations under bipolar operation. Assuming this ion concentration and a charger residence time of 11 ms at 0.3 L/min, $n{\cdot}t$ value for our charger is estimated to be $9 \times 10^5$ s/cm$^3$. This is slightly larger than the $n{\cdot}t$ value of $8.2 \times 10^5$ s/cm$^3$ estimated above based on the fitting of Fuchs numerical modeling to measured charging efficiency (in unipolar operation). Both of these estimated $n{\cdot}t$ values are much larger than the $n{\cdot}t$ value of $2.5 \times 10^5$ s/cm$^3$, which Liu et al. (1986) noted to be a lower limit for obtaining equilibrium distribution (for particles with 0 or 1 preexisting charge) in a bipolar atmosphere in a $Po^{210}$ charger.

A similar limiting $n{\cdot}t$, can be derived for our charger using the data in Figure 4, which shows the onset of nonequilibrium charging behavior at around 1.5 L/min, corresponding to a minimum flow residence time ($t_{min}$) of 2.2 ms. At 1.5 L/min, an average ion concentration of $9.0 \times 10^7$ per cm$^3$ is estimated assuming the ion concentration in the flow cavity remains the same under different flow rates. Using the $t_{min}$ value of 2.2 ms, the limiting $n{\cdot}t$ value is calculated to be $2.0 \times 10^5$ s/cm$^3$ which is within about 20% of the limiting value of $2.5 \times 10^5$ s/cm$^3$ of Liu et al. (1986) noted above. This further suggests that the actual bipolar ion concentration could perhaps be higher than the arbitrarily assumed (i.e., with respect to the bipolar operation) value above.

Assuming a bipolar ion concentration of $8.2 \times 10^7$ per cm$^3$ noted above, an approximate estimate of the minimum residence time required to achieve steady-state equilibrium distribution can be obtained using Gunn's equation (Gunn 1954), $t = 1/4\pi neZ$ (Liu and Pui 1974), where $n$ is the bipolar ion concentration, $e$ is the elementary charge, and $Z$ is the ion

mobility (in cgs units). Using the average of positive and negative ion mobilities of 1.33 and 1.84 $cm^2/V$ s (Hoppel and Frick 1990), this minimum residence time was calculated to be 4.25 ms. The charger residence time of 11 ms (at 0.3 L/min) for our charger is adequately higher than the above minimum value.

In the context of neutralization of supercharged particles, Liu and Pui (1974) noted that a minimum $n \cdot t$ value on the order of $6 \times 10^6$ $s/cm^3$ is necessary to neutralize highly charged aerosol near Rayleigh charge limit. This minimum required $n \cdot t$ value is higher by a factor of 6.7 compared to that estimated above for our charger, implying that the current charger residence time may be inadequate to "neutralize" supercharged aerosol near Rayleigh limit. However, most atmospheric and industrial aerosols have native charge distribution relatively closer to equilibrium value than the Rayleigh limit; therefore, our charger, operated with the current configuration, is expected to provide adequate charge-conditioning for these aerosols. Furthermore, the residence time of the charger can be readily increased (without increasing the overall size and complexity) by a factor of 5–10 through straightforward modification of the existing geometry (for instance by increasing the residence time of the ion-mixing region).

Though we have not investigated the charger performance as a function of aerosol concentration, aerosol with total concentrations up to $10^7$ per $cm^3$ could be satisfactorily charge-conditioned (Figure 7 and S4). The ratio of ion to particle number concentration plays an important role in this context. Adachi et al. (1989) showed that a ratio larger than about 100, 15, and 1 are necessary to attain equilibrium charge distribution for particles of diameter 1000, 100, and 10 nm. Using an estimated bipolar ion concentration of $8.2 \times 10^7$ per $cm^3$ and using the ion-to-particle number concentration ratios of Adachi et al. (1989), one can obtain limiting values of aerosol number concentration at a given size, above which our charger may not perform adequately due to ion depletion.

As with any corona-based charger, ozone generation is perhaps the key drawback of our charger. Though the measured levels of ozone (540 ppb) at the outlet of the charger were high, the total ozone release and the resulting ambient levels are not alarmingly high with respect to typical exposure timescales in indoor environments. For example, a continuous release of 540 ppb ozone at 0.3 L/min corresponds to a cumulative ambient concentration of only 2.9 ppb ozone in a room measuring $3 \times 3 \times 3$ $m^3$ (under well-mixed conditions without ventilation), if the charger is operated continuously over a period of 8 h. The resulting ozone concentrations are much lower than the OSHA PEL of 100 ppb and EPA NAAQS standard of 75 ppb, though the localized concentrations may exceed these limits in case of poor mixing. Further reduction in ozone release, if necessary, can be achieved by operating the charger at lower corona current. Being a closed system, an ozone scrubber cartridge can also be used to reduce ozone release from the instrument unit before venting to the atmosphere. Efficient electrode design, for instance by using carbon fiber electrodes (Han et al. 2009) or smaller electrode diameter (Nashimoto 1988; Boelter and Davidson 1997), has also been shown to drastically reduce ozone formation in the corona and can be further explored.

## 5. Conclusions

A miniature corona-based charger for bipolar charging of aerosols has been developed for use in compact field-portable mobility size spectrometers. Charge distributions of particles in the submicrometer range were reproducible and well-defined; they closely agreed with the theoretical equilibrium distributions. The overall transmission efficiency of the charger was found to be excellent at a low flow rate of 0.3 L/min. The charger operation was robust; the charger performance was relatively insensitive to variations in corona current in each corona ionizer. The residence time of 2.2 ms, corresponding to flow rate of 1.5 L/min at 5 $\mu$A, was established as the limiting residence time for the onset of nonequilibrium charge distributions for the current charger design. Mobility size distributions of polydisperse aerosols obtained using our charger closely agreed with those from the radioactive ionizer and a soft X-ray charger. Based on polydisperse size distribution measurement, the charger appears to be capable of neutralizing aerosol with total number concentrations up to $10^7$ per $cm^3$; though further studies will be necessary to probe the effect of aerosol concentration. The estimated $n{\cdot}t$ product value of $8.5 \times 10^5$ $s/cm^3$ (under unipolar operation) is likely adequate for neutralization of most aerosols; it can be further readily increased, if needed, by increasing the charger residence time without increasing overall size of the charger. Unlike radioactive ionizers, the DCBC is not subject to regulatory restrictions and allows access to most field measurement applications. The simple design also offers the potential for exploring low-cost fabrication alternatives using 3D prototyping or micro fabrication techniques. The miniature size, simple, and robust operation make the charger suitable for compact field-portable mobility size spectrometers for submicrometer aerosol measurement.

## Acknowledgments

The authors wish to acknowledge the review and helpful comments from Dr. Lee Turkevich and Gregory Deye.

## References

Adachi M, Okuyama K, Kousaka Y, Kozuru H, Pui DYH. Bipolar Diffusion Charging of Aerosol Particles Under High Particle/Ion Concentration Ratios. Aerosol Sci Technol. 1989; 11:144–156.

Adachi M, Pui DYH, Liu BYH. Aerosol Charge Neutralization by a Corona Ionizer. Aerosol Sci Technol. 1993; 18:48–58.

Bequin P, Castor K, Scholten J. Electric Wind Characterisation in Negative Point-to-Plane Corona Discharges in Air. Eur Phys J-Appl Phys. 2003; 22:41–49.

Boelter KJ, Davidson JH. Ozone Generation by Indoor, Electrostatic Air Cleaners. Aerosol Sci Technol. 1997; 27:689–708.

Covert D, Wiedensohler A, Russell L. Particle Charging and Transmission Efficiencies of Aerosol Charge Neutralizers. Aerosol Sci Technol. 1997; 27:206–214.

Flagan, RC. Electrical Mobility Methods for Submicrometer Particle Characterization. In: Kulkarni, P.; Baron, PA.; Willeke, K., editors. Aerosol Measurement: Principles, Techniques, and Applications. John Wiley and Sons; New York, NY: 2011.

Fuchs NA. On the Stationary Charge Distribution on Aerosol Particles in a Bipolar Ionic Atmosphere. Geofisica Pura e Applicata. 1963; 56:185–193.

Gunn R. Diffusion Charging of Atmospheric Droplets by Ions, and the Resulting Combination Coefficients. J Meteor. 1954; 11:339–347.

Gunn R. The Ratio of the Positive and Negative Light Ion Conductivities Within a Neutral Aerosol Space. J Colloid Sci. 1956; 11:661–696.

Han B, Hudda N, Ning Z, Kim HJ, Kim YJ, Sioutas C. A Novel Bipolar Charger for Submicron Aerosol Particles Using Carbon Fiber Ionizers. J Aerosol Sci. 2009; 40:285–294.

Hoppel WA, Frick GM. Ion-Aerosol Attachment Coefficients and the Steady-State Charge Distribution on Aerosols in a Bipolar Ion Environment. Aerosol Sci Technol. 1986; 5:1–22.

Hoppel WA, Frick GM. The Nonequilibrium Character of the Aerosol Charge-Distributions Produced by Neutralizers. Aerosol Sci Technol. 1990; 12:471–496.

Keefe D, Nolan PJ, Rich TA. Charge Equilibrium in Aerosols According to the Boltzmann Law. Proc R Ir Acad. 1959; 60A:27.

Kwon SB, Fujimoto T, Kuga Y, Sakkurai H, Seto T. Characteristics of Aerosol Charge Distribution by Surface-Discharge Microplasma Aerosol Charger (SMAC). Aerosol Sci Technol. 2005; 39:987–1001.

Liu BYH, Pui DYH. Electrical Neutralization of Aerosols. J Aerosol Sci. 1974; 5:465–472.

Liu BYH, Pui DYH. On the Performance of the Electrical Aerosol Analyzer. J Aerosol Sci. 1975; 6:249–264.

Liu BYH, Pui DYH, Lin BY. Aerosol Charge Neutralization by A Radioactive Alpha-Source. Particle Characterization. 1986; 3:111–116.

Nashimoto K. The Effect of Electrode Materials on O-3 and Nox Emissions by Corona Discharging. J Imaging Sci. 1988; 32:205–210.

Qi C, Kulkarni P. Unipolar Charging Based, Hand-held Mobility Spectrometer for Aerosol Size Distribution Measurement. J Aerosol Sci. 2012; 49:32–47.

Romay FJ, Liu BYH, Pui DYH. A Sonic Jet Corona Ionizer for Electrostatic Discharge and Aerosol Neutralization. Aerosol Sci Technol. 1994; 20:31–41.

Shimada M, Han BW, Okuyama K, Otani Y. Bipolar charging of aerosol nanoparticles by a soft X-ray photoionizer. J Chem Eng Jpn. 2002; 35:786–793.

Stommel YG, Riebel U. A New Corona Dischrge-Based Aerosol Charger for Submicron Particles with Low Initial Charge. J Aerosol Sci. 2004; 35:1051–1069.

Wiedensohler A. An Approximation of the Bipolar Charge Distribution for Particles in the Submicron Range. J Aerosol Sci. 1988; 19:387–390.

Wiedensohler A, Lutkemeier E, Feldpausch M, Helsper C. Investigation of the Bipolar Charge-Distribution at Various Gas Conditions. J Aerosol Sci. 1986; 17:413–416.

Withers RS, Mecher JR. Space-Charge Effects in Aerosol Charging and Migration. J Aerosol Sci. 1981; 12:307–332.

Zamorani E, Ottobrini G. Aerosol Particle Neutralization to Boltzmann's Equilibrium by a. c Corona Discharge J Aerosol Sci. 1978; 9:31–39.

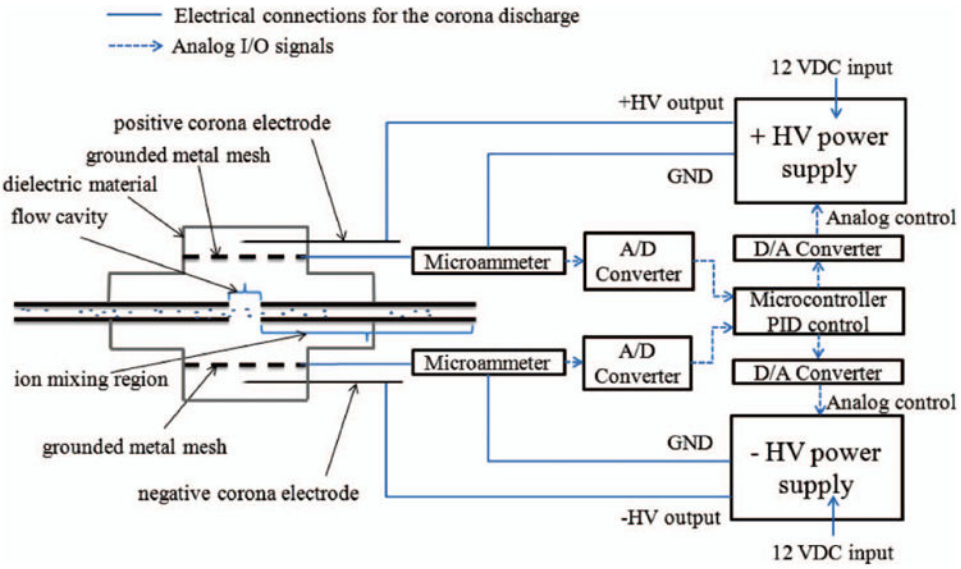


**Fig. 1.**

Schematic diagram of the DCBC and the circuit used to operate the corona ionizers. (Color figure available online.)

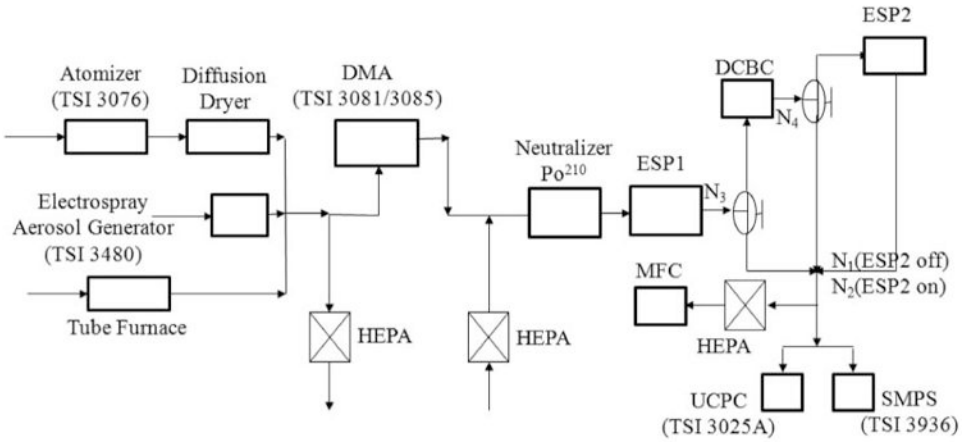


**Fig. 2.**

Schematic diagram of the experimental setup used for characterization of the DCBC.

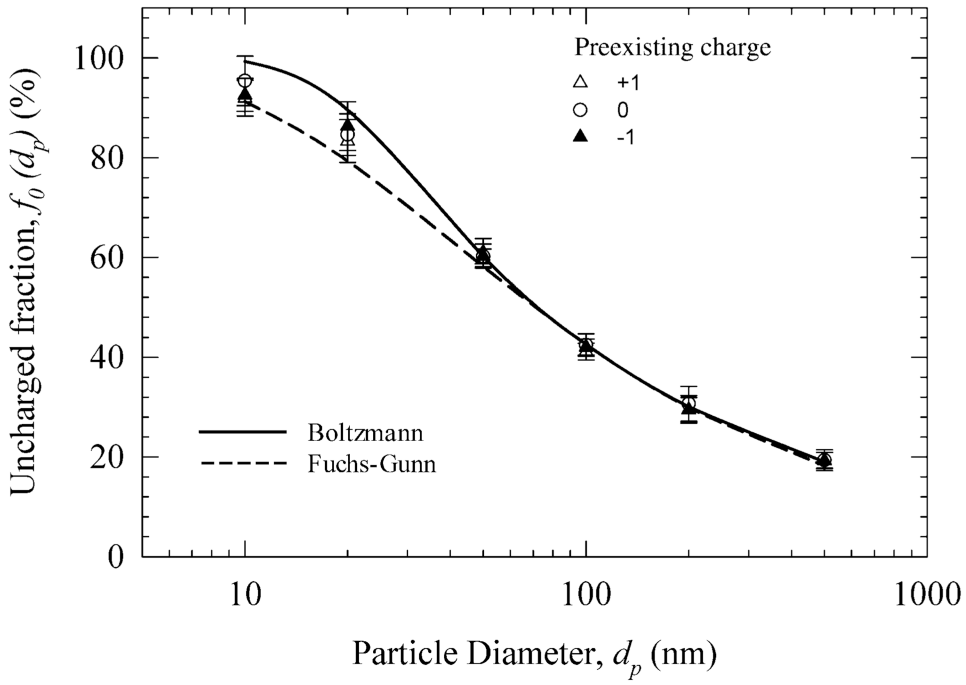


**Fig. 3.**

Uncharged fraction of test particles as a function of particle size. Positive and negative corona currents: +5 and −5 $\mu$A; aerosol flow rate = 0.3 L/min.

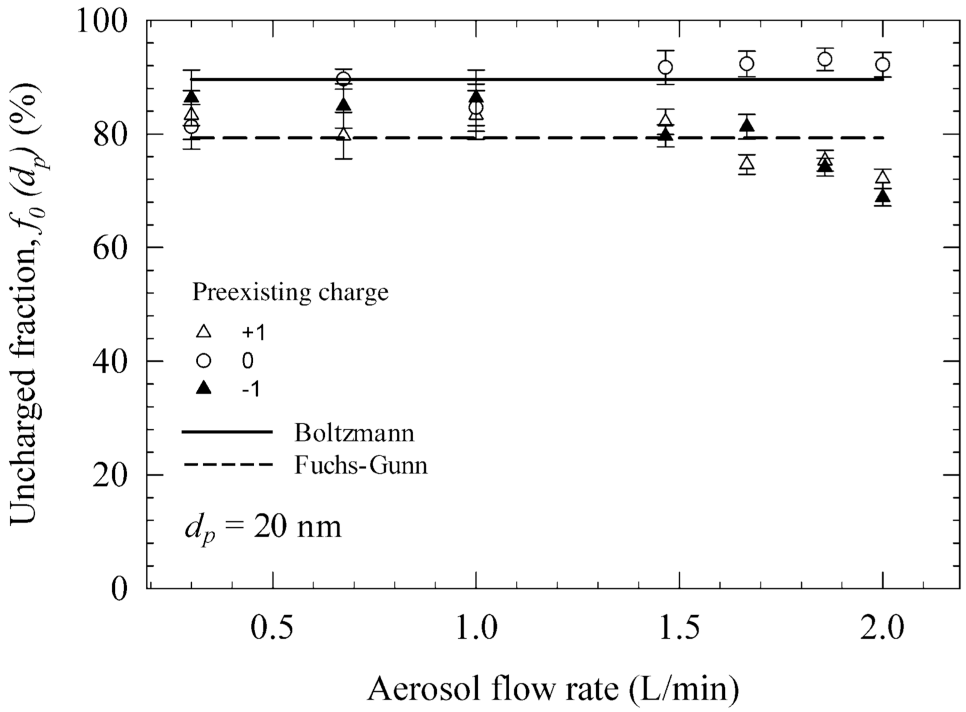


**Fig. 4.**

Uncharged fraction of 20 nm particles as a function of aerosol flow rate. Positive and negative corona currents: 5 and −5 $\mu$A.

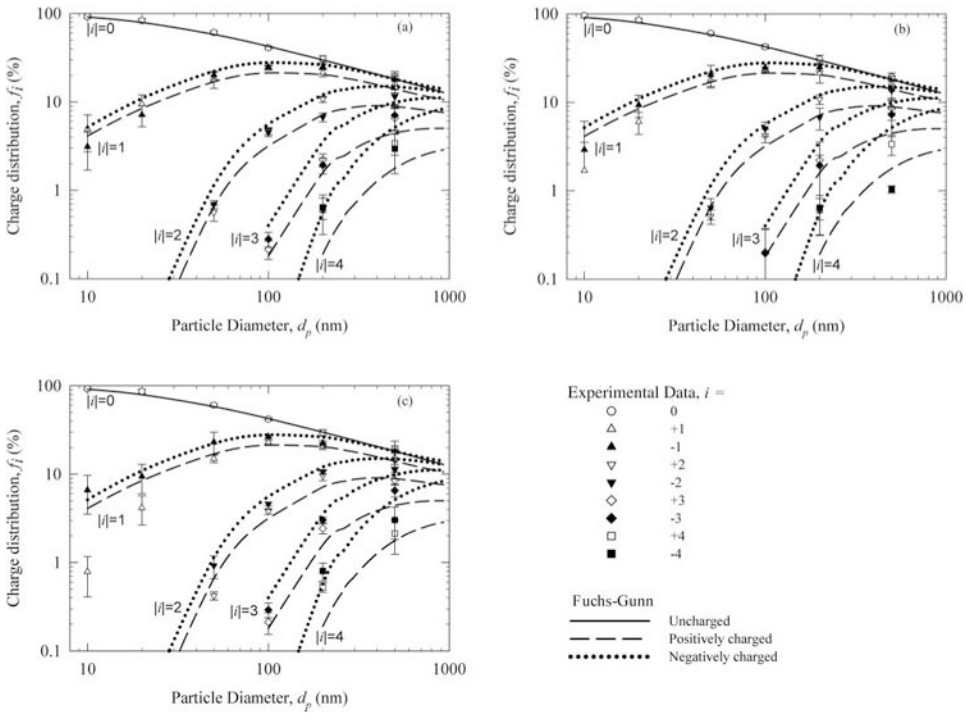


**Fig. 5.**

Charge distribution for submicrometer particles obtained from our charger: (a) positive preexisting charge; (b) zero preexisting charge (uncharged); and (c) negative preexisting charge.

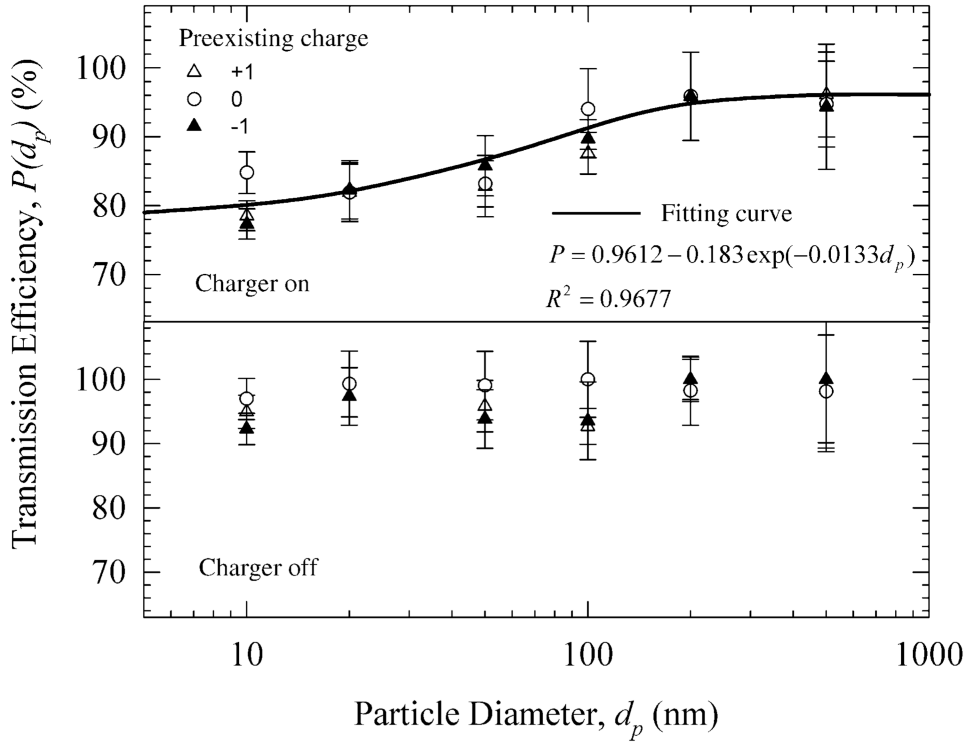


**Fig. 6.**

Transmission efficiency of the DCBC as a function of particle size. Positive and negative corona currents: 5 and −5 $\mu$A; aerosol flow rate = 0.3 L/min.

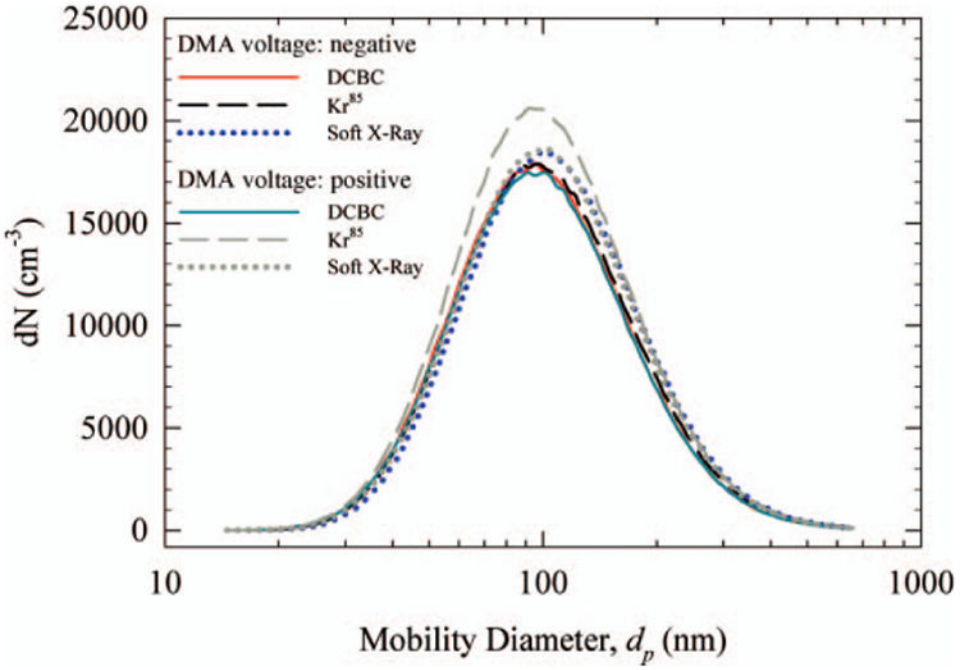


**Fig. 7.**

Size distributions obtained using different neutralizers for aerosol with no preexisting charge. Positive and negative corona currents: 5 and −5 $\mu$A; aerosol flow rate = 0.3 L/min. (Color figure available online.)

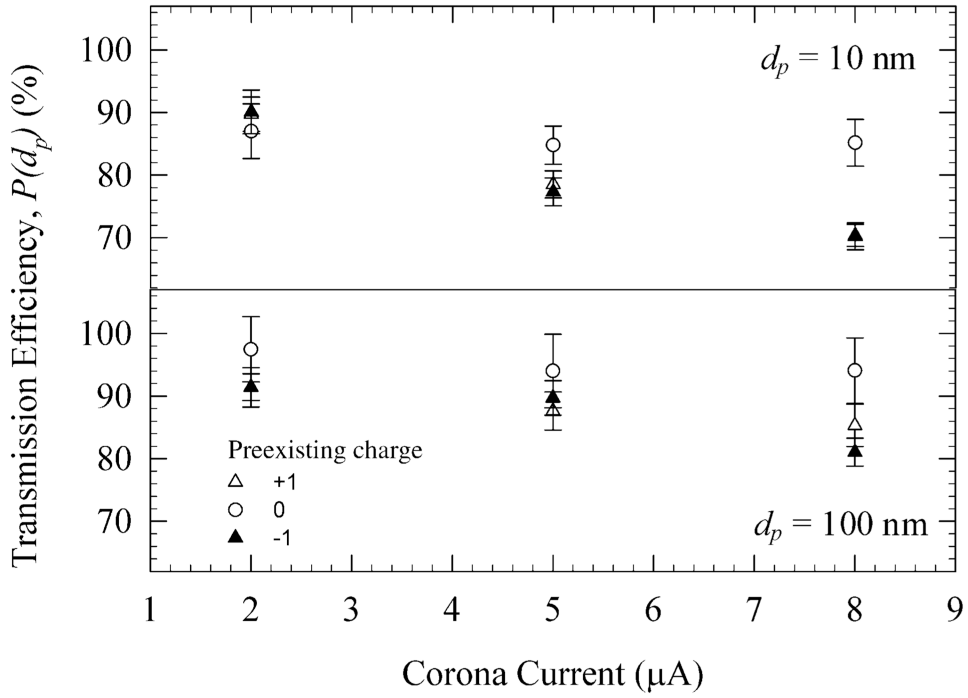


**Fig. 8.**

Transmission efficiency of the DCBC under different operating corona currents (a) 10 nm; (b) 100 nm. Flow rate = 0.3 L/min.

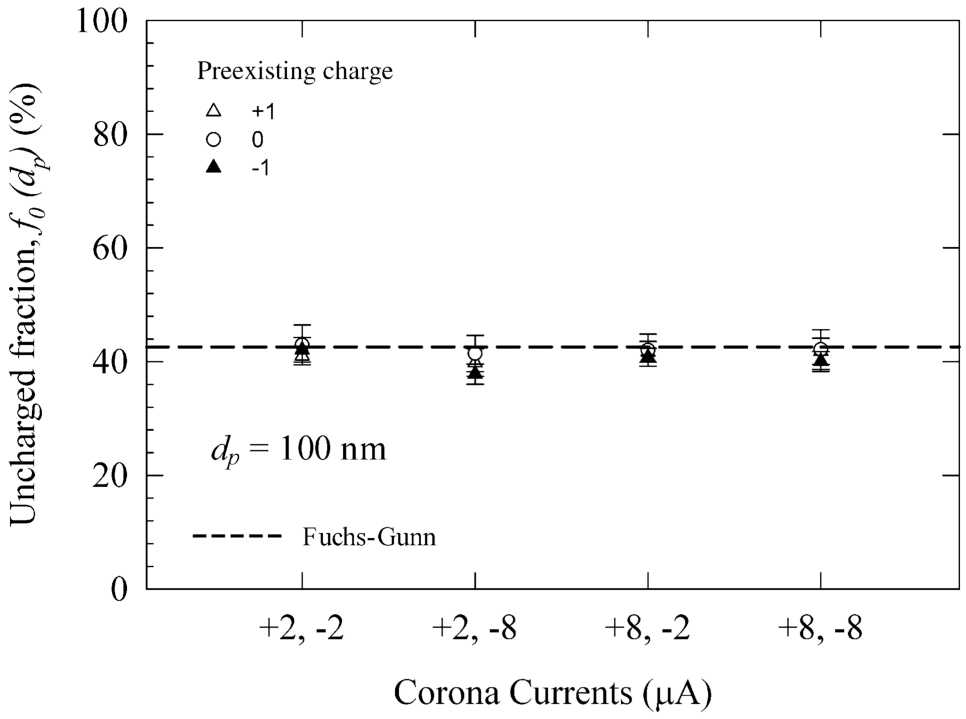


**Fig. 9.**

Uncharged fraction of 100 nm test particles (with −1, 0, and +1 preexisting charges) corresponding to different configurations of positive and negative corona currents. Flow rate = 0.3 L/min.